Density functional theory study of the γ-MnOOH (010) surface: Response to oxygen and water partial pressures and temperature

Gloria A. E. Oxford and Anne M. Chaka

Physical Measurement Laboratory, National Institute of Standards and Technology, Gaithersburg, Maryland 20899, USA

(Received 24 June 2011; revised manuscript received 16 September 2011; published 30 November 2011)

Ab initio thermodynamics was combined with density functional theory calculations to identify stable γ-MnOOH (010) surface terminations in response to varying oxygen and water partial pressures. Within the range of accessible oxygen chemical potentials, reduced manganese atoms are not thermodynamically stable at the surface. Oxidation of the surface by addition of oxygen is favorable at oxygen chemical potentials typically found in experiments. Entropy drives the removal of H_2 from the stoichiometric surface above 603 K under ambient conditions, in close agreement with the experimental decomposition temperature of 573 K. Molecular adsorption of water at half-monolayer and monolayer coverages is highly exothermic and significantly lowers the surface free energy of the clean surface. Dissociative adsorption of water is only possible at monolayer coverage, where it is stabilized by the formation of a hydrogen-bonding network on the surface. The most thermodynamically stable surfaces are oxidized surfaces, but the stoichiometric and fully hydrated surfaces may be accessible in experiments due to slow oxidation kinetics of the surface.

DOI: 10.1103/PhysRevB.84.205453 PACS number(s): 68.47.Gh, 68.43.Bc, 68.35.Md

I. INTRODUCTION

Manganese oxides represent an important class of materials that show promise in a variety of technological applications, ranging from catalysis and batteries to water treatment and sensing.[1–9] Because they are prevalent in geological settings and have significant adsorption capacity, they also play a critical role in the geochemical cycling of heavy metals.[10–14] Of particular interest is the ability of manganese oxides to oxidize heavy metal ions, including Cr^{III}[11,15–21] and As^{III}.[12,22–25] In the environment as well as in technological applications, knowledge of the structural and chemical properties of manganese oxide surfaces is essential as they are closely linked to the surface reactivity. Molecular-level understanding of these surfaces, however, is limited.

γ-MnOOH, also known as manganite, has been the subject of numerous investigations, especially in the context of electrochemical applications and heavy metal adsorption and oxidation. It is the most stable MnOOH polymorph and is pseudomorphous to rutile-type β-MnO_2. It is composed of edge-sharing $Mn^{III}O_6$ octahedra linked by shared corners. Early structural refinements placed γ-MnOOH in the $B2_1/d$ space group (Number 14) with eight formula units per unit cell.[26,27] More recently, Kohler *et al.*[28] solved the structure in the $P2_1/c$ space group (Number 14), which has only four formula units per unit cell. These two structural definitions give the same atomic arrangements. In γ-MnOOH, two distinct oxygen types are observed. The first of these, O1, is covalently bonded to the hydrogen atoms, while the second oxygen type, O2, hydrogen bonds to the hydrogen atoms. The covalent O-H bonds are arranged antiferroelectrically (AFE) in the bulk, with every other OH group aligned in the opposite direction. The tetrahedral coordination sphere of both oxygen types is completed by three manganese atoms. Each $Mn^{III}O_6$ octahedron has three O1 and three O2 atoms in its first coordination shell, with O1 and O2 forming linear O1-Mn-O2 arrangements.

Several experimental techniques have been applied to γ-MnOOH surfaces in an effort to understand the surface structure. Perfect cleavage occurs at the (010) surface, and good cleavage can be obtained at the (110) and (001) surfaces as well. High-resolution transmission electron microscopy studies performed on ion-thinned samples of natural manganite showed that the (010) and (001) surfaces are generally uniform in appearance and mostly defect-free.[29,30] Jun and Martin[31] investigated dissolution of the γ-MnOOH surface as a function of *p*H and reductant concentration and used atomic force microscopy to monitor changes in surface morphology. The single-crystal surfaces under study were determined to be predominantly the (010) surface. Before treatment, the surfaces were flat with step edges. Dissolution occurred through step retreat and etching. Above a *p*H of approximately 5.5 with O_2 present, surface precipitation competed with surface dissolution, and hillocks formed on the surface.

Surface composition has been explored in a number of experimental efforts. It is well known that γ-MnOOH oxidizes to β-MnO_2 in natural systems,[29,30,32,33] and it might be expected that Mn^{IV} may exist at the surface under certain conditions. For example, electron energy loss spectroscopy in scanning transmission electron microscopy analysis of a natural powdered sample of γ-MnOOH gave an average valence of 3.4 due to the presence of β-MnO_2.[34] X-ray photoelectron spectroscopy (XPS) has commonly been employed to determine the oxidation state of manganese at the manganite surface. Jun and Martin[31] found only Mn^{III} at the (010) surface during reductive dissolution and surface precipitation. Nesbitt and Banerjee[35] also analyzed single crystals and detected Mn^{III} at the surface, but the exposed surface was not identified. In other XPS studies, powdered samples were used, and therefore, it is unclear as to which surfaces contributed to the results. Mn^{III} was observed in some cases,[36,37] while Mn^{IV} was detected by Ramstedt *et al.*[38] after acid treatment. Oku *et al.*[39] were unable to assign an unambiguous valence to manganese in γ-MnOOH because partial dehydration of the sample occurred at room temperature in their vacuum system. Some of the XPS experiments also examined the nature of oxygen at the manganite surface. A few reports have shown the OH^-:O^{2-}

ratio at the surface to be close to 1:1.[35,36] One investigation demonstrated that the OH^-:O^{2-} ratio increased with *p*H, possibly as a result of deprotonation of surface-bound water.[38] Nesbitt and Banerjee[35] identified structurally or chemisorbed water in the O 1*s* spectra as did Ramstedt and co-workers.[38] Again, it is unknown which surfaces were relevant in these reports.

Although the small number of surface studies described here offers some information for building a γ-MnOOH surface model, there exist significant gaps in the molecular-level detail that need to be addressed in order to probe chemical properties and redox behavior of these surfaces. Atomistic modeling using density functional theory (DFT) has become a reliable method for examining various surface terminations and finding stable reconstructions that can be used in the interpretation of experimental data.[40–43] Recently, Xia *et al.*[44] applied DFT and *ab initio* molecular dynamics (AIMD) to explore the perfect (010) cleavage surface of manganite and the effect of hydration on surface structure. The clean stoichiometric surface was found to be stable and to exhibit electronic properties similar to the bulk. Water physisorbed on the surface, but dissociated water could not be stabilized. It was concluded that the local water environment controlled the surface structure and water-water interactions were stronger than the water-surface interactions, especially when liquid water was simulated at the surface. While this study thoroughly addressed surface hydration, the redox behavior of the surface was not investigated. Here, we present DFT calculations of reduced and oxidized γ-MnOOH (010) surfaces and compare their thermodynamic stability to the stability of clean stoichiometric and hydrated surfaces under varying oxygen and water partial pressures across a range of temperatures. Reduction of the surface is not favorable, but surface oxidation results in thermodynamically stable surface reconstructions. Although surface hydration significantly lowers the surface energy compared to the clean surface, the lowest-energy hydrated surface is metastable to the fully oxidized surface. Our results indicate that most experimental work may have observed unoxidized and kinetically trapped metastable surfaces.

II. METHODS

A. DFT calculations and method validation

Periodic DFT calculations were performed using standard density functional software.[45,46] The generalized gradient approximation (GGA) formalism of Perdew *et al.*[47] was utilized with a double-numeric-plus-polarization atom-centered basis set. The $P2_1/c$ structure of Kohler *et al.*[28] with four formula units per unit cell was used. Bulk lattice optimizations were carried out using $(3 \times 3 \times 3)$ *k* points in a Monkhorst-Pack grid[48] and a real-space cutoff of 4.5 Å. Possible spin arrangements for $P2_1/c$ manganite include nonmagnetic (NM), ferromagnetic (FM), and three antiferromagnetic (AFM) states ($+--+$, $++--$, $+-+-$). All AFM structures are lower in energy than the NM and FM structures, in agreement with experimental evidence of the AFM character of γ-MnOOH below 45 K.[49] Specifically, the $+--+$ structure is the most stable followed by the $++--$, $+-+-$, FM, and NM configurations with energies of 2.1, 52, 125, and 385 meV per formula unit, respectively, relative to the $+--+$ structure. The $+--+$ and $++--$ configurations are close in energy because, in the (010) plane, each manganese is surrounded by manganese atoms of the opposite spin (the spins alternate along the [101] and [$\bar{1}$01] directions). They differ only in that the $+--+$ structure has an AFM arrangement of spins in the (001) plane, while the $++--$ structure exhibits an FM spin arrangement in this plane.

The optimized bulk lattice constants and bond lengths for the AFM $+--+$ and FM structures are compared to other DFT-GGA results and to experimental data in Table I. Generally, the AFM configuration gives better agreement with experimental data than the FM structure, as expected, but the calculated FM bulk lattice constants are only 0.69% and 0.50% larger than the AFM ones. Excellent agreement with the experimental bulk lattice constants[28] is achieved for the AFM structure with calculated values of 5.357 Å (+1.0%) and 5.330 Å (+1.0%) (percent error shown in parentheses). Bond lengths are overestimated by no more than 2% for the Mn-O bonds and 4% for the O-H bonds and are in good agreement with other DFT-GGA results[44,50] (Table I). The magnitude of the spins for the AFM $+--+$ configuration is determined to be $3.73\mu_B$ and $3.45\mu_B$ by the Mulliken and Hirshfeld methods, respectively, which is higher than the experimental spin moment of $3.3\mu_B$.[49]

The manganite band gap has not been measured experimentally. A band gap of 1.16 eV is calculated for the most stable structure, but it is likely that the band gap is underestimated, a known problem in DFT-GGA calculations due to the DFT self-interaction error. A number of methods have been used to correct this error, including the DFT + *U* approach[51] and hybrid functionals.[52] Arguments for using these methods to model manganese oxides are based on the highly correlated nature of these systems and on the ability of these methods to correctly predict the band gap of MnO.[53–56] However, it is uncertain how well these methods will predict surface energies for these systems given the lack of experimental data with which to compare calculated results. In fact, Franchini *et al.*[56] found that DFT + *U* and hybrid functionals both give incorrect trends for relative formation energies for a number of manganese oxides, with oxygen-poor compounds being overstabilized compared to the oxygen-rich ones. While GGA underestimates formation energies, it predicts the correct trend. Because we are interested in relative energies of surfaces with varying amounts of oxygen, GGA should be the most reliable method for this system.

The (010) surface model was constructed from the optimized bulk AFM $+--+$ structure, maintaining the spin ordering throughout the slab. The surfaces of the slab were related by inversion symmetry and were separated by at least 10 Å of vacuum. A (1×1) surface cell with a surface area of 26.1 $Å^2$ was used for all calculations. For the stoichiometric surface termination, the (1×1) surface consists of one O1 atom and one O2 atom in the first atomic layer and two exposed manganese atoms in the second atomic layer [see Fig. 1(a) for the layer sequencing]. The slab was treated with a $(3 \times 1 \times 3)$ Monkhorst-Pack grid.[48] The real-space cutoff was reduced to 3.5 Å for computational efficiency, but increasing the real-space cutoff to 5.5 Å led to a difference of no more than a few meV/$Å^2$ in surface free energy γ. All atoms in

TABLE I. Theoretical and experimental lattice constants as defined in the $P2_1/c$ space group and bond lengths for bulk γ-MnOOH AFM and FM states.

Method	Spin ordering	a (Å)	b (Å)	c (Å)	β (degree)	$R_{\text{Mn-O1}}$ (Å)	$R_{\text{Mn-O2}}$ (Å)	$R_{\text{O1-H}}$ (Å)	$R_{\text{O2-H}}$ (Å)
DFT-GGA	AFM	5.357	5.330	5.357	114.38	2.006	1.895	1.017	1.604
						2.015	1.900		
						2.363	2.229		
DFT-GGA	FM	5.394	5.356	5.394	114.38	2.006	1.912	1.020	1.610
						2.019	1.927		
						2.405	2.223		
DFT-GGA (Ref. 50)	FM	5.309	5.279	5.317	112.90	1.986	1.947	1.114	1.360
						1.991	1.955		
						2.319	2.227		
DFT-GGA (Ref. 44)[a]	AFM	5.330	5.348	5.330	113.53	1.99	1.89	1.028	1.552
						2.00	1.91		
						2.39	2.25		
XRD (Ref. 26)[a]	AFM	5.27	5.24	5.27	114.49	1.92	1.85		
						2.30	2.30		
XRD/ND (Ref. 27)[a]	AFM	5.28	5.25	5.28	114.52	1.965	1.862	1.022	1.561
						1.981	1.884		
						2.333	2.196		
XRD (Ref. 28)	AFM	5.304	5.277	5.304	114.38	1.977	1.881	0.98	1.61
						1.982	1.893		
						2.337	2.213		

[a]Redefined from $B2_1/d$ space group lattice constants.

the slab were optimized using a force tolerance of 0.01 eV/Å. Optimal slab thickness was determined by convergence of γ and comparison of the geometries of the central layers to calculated bulk geometries. At five metal layers, γ is well converged as are the geometries in the middle of the slab.

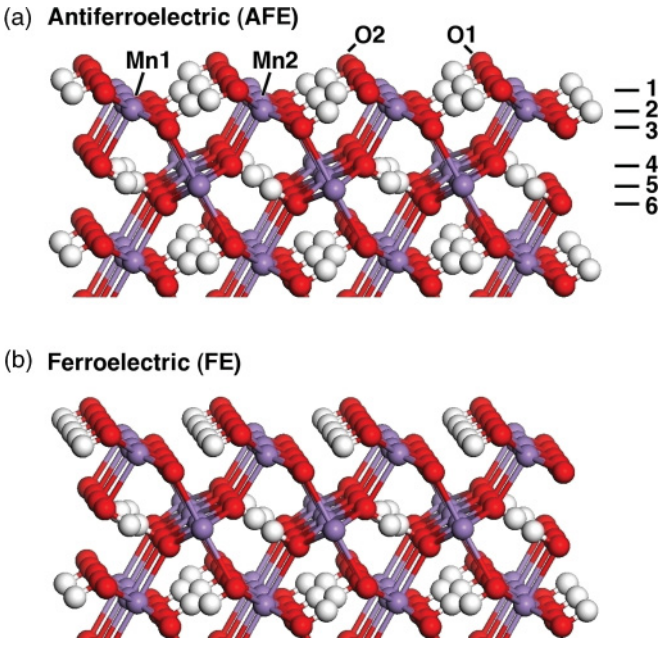

FIG. 1. (Color online) γ-MnOOH (010) stoichiometric surfaces viewed along the [101] direction demonstrating the (a) AFE and (b) FE orientations of the O-H bonds at the surface. The vertical layer sequence and the surface atom types are shown in (a). [Mn, purple (light) sphere; O, red (dark) sphere; H, white sphere].

Oxidation states of the manganese atoms were calculated using the Mulliken and Hirshfeld spins, which indicate the number of unpaired electrons on the atoms, and knowledge of the number of electrons in the system relative to the stoichiometric surface. The frozen phonon method[57] was employed in frequency calculations with perturbation of atom positions by ±0.53 pm (0.01 bohr) in each direction.

B. *Ab initio* thermodynamics

To extend surface energy values calculated at 0 K to experimentally relevant temperatures and pressures, *ab initio* thermodynamics was employed. This theoretical framework has become an increasingly popular method for identifying dominant surface terminations under variable temperatures and pressures.[40,41,43,58–67] For a system at equilibrium under constant temperature and pressure, the thermodynamic behavior is governed by the relationship between Gibbs free energy, enthalpy, and entropy: $G = H - TS$. Here, we assume chemical and thermal equilibriums exist between the surface, the bulk, and a gas reservoir. The following equation then defines γ as a function of temperature and pressure,

$$\gamma(T,p) = \frac{1}{2A}\left\{G_{\text{slab}}(T,p,N_i) - \sum_i N_i \mu_i(T,p)\right\}. \quad (1)$$

In Eq. (1), G_{slab} is the Gibbs free energy of the slab, and N_i and μ_i are the number and chemical potential, respectively, of type i atoms. The total Gibbs free energy is divided by twice the surface area to account for two equivalent surfaces of the slab.

The Gibbs free energy of the slab can be calculated by considering the contributions at 0 K and at higher temperatures separately. At 0 K and pressures below 10.1 MPa, the enthalpy

is essentially equivalent to the internal energy of the system,[60] which is simply the DFT total energy of the slab neglecting the zero-point energy. The enthalpic and entropic contributions at finite temperatures are encompassed in the change in Gibbs free energy due to vibrational energy (including the zero-point energy) for the slab as well as for the bulk oxide. For these two components of the system, calculation of the vibrational component to the free energy involves the mathematical framework of statistical mechanics. Details can be found in the thorough treatment by McQuarrie.[68] Here, we present only the final equation for the calculation of the change in Gibbs free energy due to vibrational energy ΔG^{vib},

$$\Delta G^{\text{vib}} = k_B \sum_i \Theta_{v_i} \left(\frac{1}{2} + \frac{1}{e^{\Theta_{v_i}/T} - 1} \right) - k_B T \sum_i \left[\frac{\Theta_{v_i}/T}{e^{\Theta_{v_i}/T} - 1} - \ln(1 - e^{\Theta_{v_i}/T}) \right]. \quad (2)$$

The summation is over all vibrational frequencies v_i, and the vibrational temperature Θ_{v_i} is equal to hv_i/k_B, where h is the Planck constant and k_B is the Boltzmann constant. The vibrational energy contribution to the Gibbs free energy is surface dependent as it is highly sensitive to the presence of OH groups. The different surface structures studied in this work lead to different magnitudes of this contribution to γ. For example, γ is lowered by 13 meV/Å^2 at 298.15 K when all surface hydrogen are removed, but full hydration of the surface with physisorbed water lowers γ by 19 meV/Å^2 at the same temperature.

Because the chemical potential of each atom type must be equal in all phases at equilibrium, μ_i can be defined in terms of the Gibbs free energies of the bulk oxide and of the gas-phase species,

$$\mu_{\text{Mn}} + 2\mu_{\text{O}} + \mu_{\text{H}} = G^{\text{bulk}}_{\text{MnOOH}}, \quad (3)$$

$$\mu_{\text{O}} = \tfrac{1}{2} G^{\text{gas}}_{\text{O}_2}, \quad (4)$$

$$\mu_{\text{H}} = \tfrac{1}{2} G^{\text{gas}}_{\text{H}_2}, \quad (5)$$

$$2\mu_{\text{H}} + \mu_{\text{O}} = G^{\text{gas}}_{\text{H}_2\text{O}}. \quad (6)$$

As with the Gibbs free energy of the slab, the chemical potentials of the elements can be determined from the DFT total energies and enthalpic and entropic contributions to the Gibbs free energy at finite temperatures. Because of the lack of relevant experimental data, these contributions to $G^{\text{bulk}}_{\text{MnOOH}}$ were computed using Eq. (2). For the gas-phase species, the change in Gibbs free energy as a function of temperature includes translational and rotational energies as well as the vibrational energy. The NIST-JANAF tables[69] provided the data for calculating the temperature dependence of μ_{O} and μ_{H}. The pressure dependence was determined using the following equation:

$$\mu_i(T,p) = \mu_i(T,p^\circ) + \frac{1}{2} k_B T \ln\left(\frac{p}{p^\circ}\right). \quad (7)$$

Physical constraints place boundaries on the range of accessible μ_{O} values. The oxygen-rich limit is characterized by condensation of O_2 on the surface, while the oxide separates into bulk metal, O_2 gas, and H_2 gas at the oxygen-poor limit. If this range of μ_{O} values is rescaled so that, in the oxygen-rich limit, μ_{O} is equal to 0 eV, the following relationship defines the range of accessible μ_{O} values:

$$\tfrac{1}{2}\left(G^{\text{bulk}}_{\text{MnOOH}} - G^{\text{bulk}}_{\text{Mn}} - G^{\text{gas}}_{\text{O}_2} - \tfrac{1}{2} G^{\text{gas}}_{\text{H}_2}\right) < \mu_{\text{O}} - \tfrac{1}{2} G^{\text{gas}}_{\text{O}_2} < 0. \quad (8)$$

The Gibbs free energy of bulk manganese metal $G^{\text{bulk}}_{\text{Mn}}$ was calculated for collinear AFM α-Mn using DFT-GGA optimized lattice constants[70] and (4 × 4 × 4) k points in a Monkhorst-Pack grid.[48] It was shown by Hobbs *et al.*[70] that a collinear spin arrangement is a good model energetically for the real noncollinear system at the optimized lattice constants. For the Gibbs free energy of O_2, we used the experimental value for the dissociation energy to correct for the well-known 0.9-eV error in the GGA energy as documented in previous studies.[43,47,67] Given that no thermochemical data exist for the heat of formation of γ-MnOOH, the calculated energies for bulk manganite, collinear AFM α-Mn, and H_2 were employed along with the corrected energy for the O_2 molecule to obtain a value of −6.68 eV for the heat of formation of γ-MnOOH at 0 K. The lower limit of μ_{O} in Eq. (8) is thus determined to be −3.34 eV.

It should be noted that μ_{O} and μ_{H} are independent variables, and surface hydrogen in equilibrium with both H_2 and H_2O need to be considered. At low oxygen concentrations, surface hydrogen atoms are in equilibrium with H_2, and Eq. (5) applies. When the oxygen partial pressure is high enough, μ_{H} is dominated by equilibrium with water and is therefore described by Eq. (6). The crossover from equilibrium with H_2 to equilibrium with H_2O as a function of μ_{O} is calculated to be −2.89 eV by solving Eqs. (5) and (6) for μ_{H} and then equating them. [This crossover is indicated by a vertical dashed line in Figs. 3(a) and 6(a).] Uncorrected values were used for H_2 and H_2O atomization energies, as the GGA errors are small, i.e., 0.13 and 0.042 eV, respectively, consistent with a previous study.[47]

III. RESULTS AND DISCUSSION

A. Clean stoichiometric surface

The γ-MnOOH (010) stoichiometric surface is depicted in Fig. 1. It consists of two types of manganese atoms, Mn1 and Mn2, which differ in the oxygen atom type in layer 4 to which they are bonded [see Fig. 1(a) for layer sequencing]. Mn1 is bonded to subsurface O1, while Mn2 bonds to subsurface O2. Each row of square pyramidal manganese along the [101] direction contains alternating Mn1 and Mn2. Similarly, the AFE surface shown in Fig. 1(a) has rows of alternating O1 and O2 atoms along the [101] direction. Mn1 and Mn2 also alternate along the [$\bar{1}$01] direction as do O1 and O2. On the ferroelectric (FE) surface [Fig. 1(b)], all O-H dipoles are oriented in the same direction. It is formed by the transfer of hydrogen atoms from O1 in layer 3 to O2 in layer 1 so that all layer 1 and layer 3 oxygen atoms are chemically equivalent to O1 and O2, respectively. Both the AFE and the FE surfaces were optimized, and the FE surface was found to be more stable than the AFE surface by approximately 3.3 meV/Å^2

TABLE II. Calculated vertical layer spacings d (Å) and percent relaxations with respect to theoretical bulk spacings for stable surface terminations of the γ-MnOOH (010) surface.

		Stoichiometric AFE		Stoichiometric FE		O = Mn AFE		O = Mn FE		2H		H_2O-Mn AFE		H_2O-Mn FE		HO-Mn	
Layers		d	%Δ	d	%Δ	d	%Δ	d	%Δ	d	%Δ	d	%Δ	d	%Δ	d	%Δ
$x-1$[a]						1.093		0.688				1.474		1.502		1.105	
						0.985		0.417				1.511		1.519		1.081	
1–2	O1[b]	0.752	+23	0.777	+27	0.288	−53	0.549	−10	0.797	+30	0.672	+10	0.713	+16	0.591	−4
	O2[c]	0.670	+9	0.763	+25	0.241	−61	0.453	−26	0.769	+26	0.650	+6	0.705	+15	0.581	−5
2–3	Mn1	0.546	−24	0.509	−29	0.968	+34	1.200	+67	0.869	+21	0.649	−10	0.599	−17	0.693	−4
	Mn2	0.499	−18	0.457	−25	0.844	+38	0.950	+55	0.736	+20	0.585	−4	0.533	−13	0.654	+7
3–4		1.397	+5	1.372	+3	1.196	−10	0.945	−29	0.912	−32	1.353	+2	1.332	0	1.173	−12
4–5		0.566	−8	0.590	−4	0.594	−3	0.588	−4	0.586	−4	0.602	−2	0.622	+2	0.690	+13
5–6	Mn1	0.737	+2	0.712	−1	0.742	+3	0.776	+8	0.792	+10	0.722	0	0.701	−3	0.712	−1
	Mn2	0.618	+1	0.673	+10	0.638	+4	0.741	+21	0.778	+27	0.618	+1	0.668	+9	0.667	+9

[a]Values in first and second rows are for O^{2-}, H_2O, or OH^- adsorbed on Mn1 and Mn2, respectively.
[b]Structurally equivalent to O1 in the bulk but chemically equivalent to O2 for the 2H and HO-Mn surfaces.
[c]Structurally equivalent to O2 in the bulk but chemically equivalent to O1 for FE surfaces.

in γ between 0 and 700 K. These results are consistent with those of Xia *et al.*,[44] who also determined that the FE surface is lower in energy than the AFE surface. The preference for the FE arrangement of O-H dipoles at the surface results from the fact that O2 is three-fold coordinated on the FE surface, whereas it is only two-fold coordinated and comparatively undersaturated on the AFE surface.

The effect of the O2 coordination number at the surface can be observed in the calculated vertical and lateral surface relaxations, which are presented in Tables II and III, respectively. Layer 1 O1 undergoes a large outward relaxation of +23% relative to the bulk on the AFE surface and +27% on the FE surface. Layer 1 O2 also expands out of the surface by +25% on the FE surface, but a significantly smaller expansion is observed on the AFE surface (+9%). Mn1 and Mn2 in layer 2 show large inward relaxations (−18% to −29%) on both surfaces, but the layer 2–3 spacing contracts less on the AFE surface (Table II). The combined effect of the smaller relaxations of layer 1 O2 and layer 2 manganese on the AFE surface is to decrease the Mn-O2 bond lengths relative to the FE surface (1.85 vs 1.95 Å). The short Mn-O2 bonds on the AFE surface allow the coordinatively unsaturated O2 atom to draw more electron density from the surface manganese atoms and to partially satisfy its undersaturation. Another noteworthy difference in the calculated vertical layer spacings between the AFE and FE surfaces is the layer 5–6 Mn2-O relaxations (+1% and +10% for the AFE and FE surfaces, respectively), which are affected by the layer 3 oxygen coordination. Specifically, the layer 3 oxygen to which layer 5 Mn2 is bonded changes from O1 on the AFE surface to O2 on the FE surface. The stronger Mn2-O2 interaction pulls Mn2 further out of the surface, and the layer 3 O-layer 5 Mn2 bond length decreases by 0.10 Å on the FE surface. Small lateral relaxations along the [001] and [100] directions are observed through layer 5 for both surfaces (Table III). The most significant lateral relaxations involve the first two layers, and generally, larger relaxations are

TABLE III. Calculated lateral relaxations (Å) with respect to theoretical bulk spacings for stable surface terminations of the γ-MnOOH (010) surface.

		Stoichiometric AFE		Stoichiometric FE		O = Mn AFE		O = Mn FE		2H		H_2O-Mn AFE		H_2O-Mn FE		HO-Mn	
Layers		[001]	[100]	[001]	[100]	[001]	[100]	[001]	[100]	[001]	[100]	[001]	[100]	[001]	[100]	[001]	[100]
1	O1[a]	+0.11	−0.05	+0.14	−0.07	+0.04	−0.08	+0.51	−0.44	+0.59	−0.33	+0.03	−0.02	+0.07	−0.03	−0.17	+0.15
	O2[b]	+0.04	−0.02	+0.09	−0.06	+0.01	+0.02	+0.53	−0.25	+0.52	−0.39	+0.01	−0.02	+0.03	−0.02	−0.21	+0.16
2	Mn1	−0.05	+0.04	+0.05	+0.05	+0.07	−0.05	+0.56	−0.32	+0.25	−0.09	−0.04	+0.02	+0.07	+0.04	−0.13	+0.17
	Mn2	−0.02	+0.01	+0.02	−0.09	+0.05	−0.01	+0.36	−0.36	+0.09	−0.17	0	−0.01	+0.04	−0.10	−0.15	+0.04
3		+0.03	−0.02	+0.06	−0.03	−0.07	+0.02	+0.05	−0.06	+0.18	−0.09	+0.01	−0.01	+0.05	−0.02	−0.11	+0.08
4		+0.01	−0.01	+0.02	−0.01	+0.01	0	+0.03	−0.03	+0.13	−0.06	+0.01	−0.01	+0.01	−0.01	+0.01	0
5	Mn1	−0.01	0	0	−0.01	+0.02	0	+0.08	−0.04	+0.10	−0.04	0	0	+0.01	−0.01	+0.02	+0.01
	Mn2	0	0	−0.03	+0.02	+0.01	0	+0.04	−0.04	+0.07	−0.01	0	0	−0.02	+0.02	−0.02	+0.01
6		0	0	0	0	+0.02	0	+0.08	−0.04	+0.12	−0.06	0	0	0	+0.01	0	+0.01

[a]Structurally equivalent to O1 in the bulk but chemically equivalent to O2 for the 2H and HO-Mn surfaces.
[b]Structurally equivalent to O2 in the bulk but chemically equivalent to O1 for FE surfaces.

observed for the FE surface due to the differences in hydrogen positions at the surface compared to those in the bulk.

Partial density of states (PDOS) calculations were performed for both the stoichiometric AFE and the FE surfaces. The resulting PDOS for the surface atoms are shown in Fig. 2 along with the PDOS of bulk γ-MnOOH. Comparison of the PDOS of the surfaces [Figs. 2(a) and 2(b)] to the PDOS of the bulk [Fig. 2(c)] illustrates the similar electronic character of the surface and the bulk and confirms the results of Xia *et al.*[44] In all cases, a band gap of approximately 1.2 eV is observed, demonstrating that no conducting states appear at the surface. Considerable overlap of the manganese 3*d* and oxygen 2*p* orbitals between 2.2 and 6.3 eV below the Fermi energy (E_F) reveals covalent bonding at the AFE and FE surfaces [Figs. 2(a) and 2(b)]. Covalent interactions within the same range are also observed in the bulk [Fig. 2(c)]. Yet, significant ionicity is also apparent as both surfaces and the bulk have significant localization of electrons in the 3*d* orbitals on manganese shown by large peaks in the manganese PDOS above −2.0 eV. Xia *et al.*[44] also reported a combination of covalent and ionic interactions between manganese and oxygen in γ-MnOOH based on analysis of atomic charges. Above −2.0 eV, the AFE surface shows more covalency than the FE surface and the bulk with good overlap between the manganese 3*d* and O2 2*p* orbitals between 0.95 and 1.5 eV below E_F [Fig. 2(a)]. The manganese 3*d* orbitals on the FE surface [Fig. 2(b)] and in the bulk [Fig. 2(c)], however, interact little with the O 2*p* orbitals within this region and shift to lower energies (between −2.0 and −1.2 eV). This difference between the AFE and the FE surface electronic structures occurs because of the short Mn-O2 bonds at the AFE surface that allow more manganese-oxygen orbital interactions. When O2 covalently bonds to hydrogen in the FE surface, the majority of the O2 2*p* PDOS above −2.0 eV shifts to the O 2*p*-H 1*s* orbital interaction

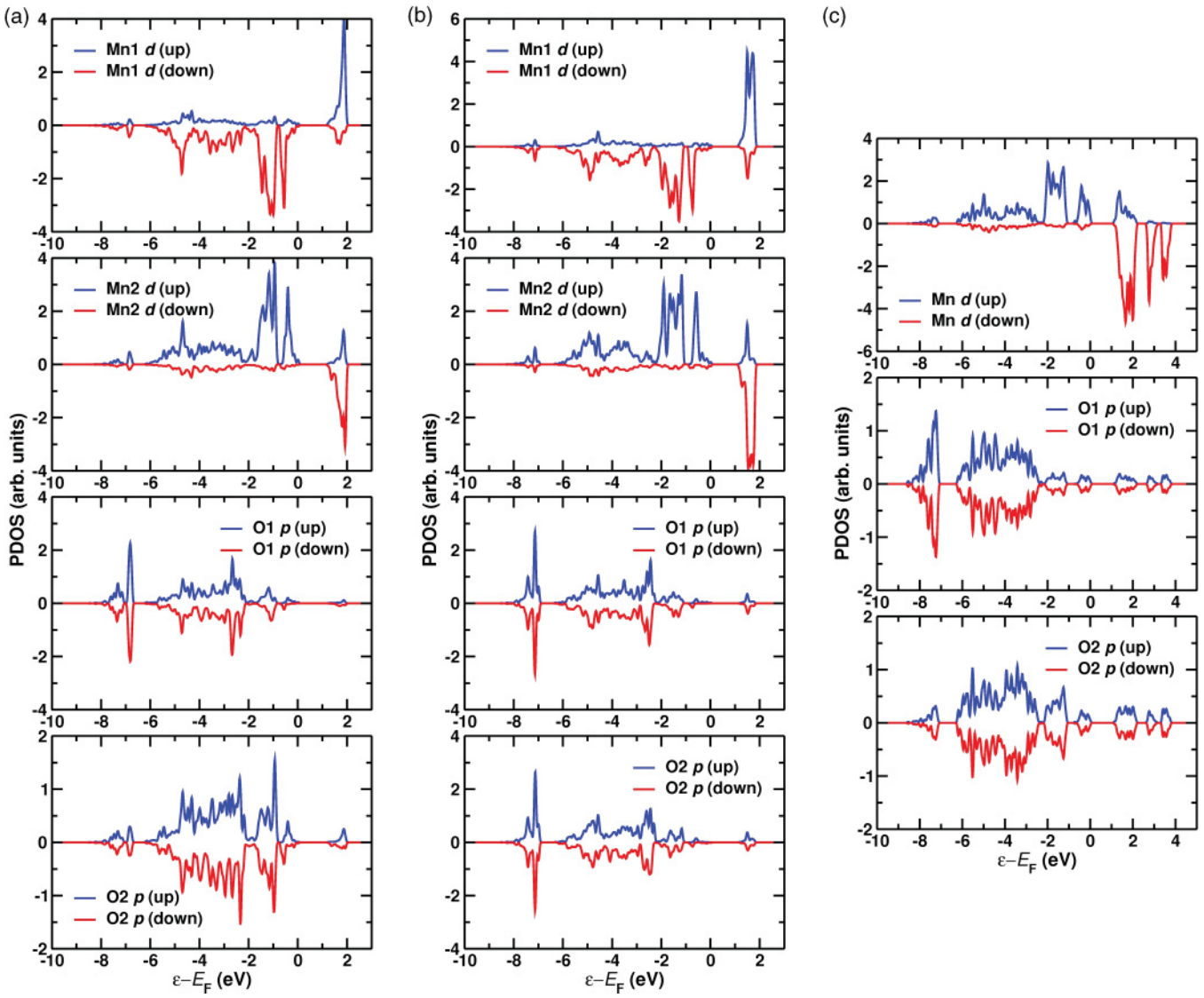

FIG. 2. (Color online) PDOS of the γ-MnOOH (010) stoichiometric (a) AFE and (b) FE surfaces and of (c) bulk γ-MnOOH. (a) and (b) (Top) Mn1 3*d*, (middle top) Mn2 3*d*, (middle bottom) O1 2*p*, and (bottom) O2 2*p*. (c) (Top) Mn 3*d*, (middle) O1 2*p*, and (bottom) O2 2*p*. In (b), O2 is structurally equivalent to O2 in the bulk but chemically equivalent to O1. Majority spin is blue (positive), and minority spin is red (negative).

region between −8.1 and −6.9 eV. For both surfaces and the bulk, additional manganese 3*d* PDOS appears above −0.75 eV. The manganese 3*d* states above −2.0 eV are due to unpaired electrons, which is consistent with the assigned oxidation state of high-spin Mn^{III} at the surface and in the bulk based on the average calculated Mulliken spins of 3.75 and 3.73, respectively.

B. Reduced and oxidized surfaces

To investigate the change in γ-MnOOH surface structure in response to varying oxygen and water partial pressures (p_{O_2} and p_{H_2O}), several chemical processes were considered that could have an impact on surface structure, including volatility of hydrogen and oxygen that would release H_2, O_2, or H_2O and would form vacancies as the temperature increases; dissociation of oxygen and water at exposed undercoordinated manganese sites; and flexible protonation states of surface oxygen atoms that can form many different hydrogen bonding networks. The surfaces constructed by removing atoms from the stoichiometric surface are labeled by the name and number of the atoms that are removed per (1 × 1) surface cell. These surfaces are O1 + H, O2, O1 + O2, O1 + H/O2, O1 + 2H, and 2H. The first four surfaces, O1 + H, O2, O1 + O2, and O1 + H/O2, are reduced. The 2H surface contains oxidized manganese atoms. Other oxidized surfaces are obtained by adding atomic oxygen to Mn1 (O = Mn1), Mn2 (O = Mn2), or both Mn1 and Mn2 (O = Mn). These nine surfaces are limiting cases that address the surface chemical processes outlined above and allow for comparison of the relative reactivities of the different types of surface atoms (e.g., Mn1 vs Mn2). For each surface, all possible arrangements of O-H dipoles at the surface were explored. Surfaces with two-fold coordinated O2 at the surface are stabilized by hydrogen transfer from layer 3 O1 to layer 1 O2 (see Fig. 1). Specifically, when vibrational energy contributions to γ are excluded, γ of O1 + H is lowered by 7.64 meV/Å^2, and the O = Mn1, O = Mn2, and O = Mn FE surfaces are preferred over the AFE surfaces by 1.41, 2.08, and 20.1 meV/Å^2, respectively.

Ab initio thermodynamics results for the lowest-energy structure of each surface are presented in Fig. 3 (both the O = Mn AFE and FE surface results are given due to the large difference in their energies). The surface free energy phase diagram in Fig. 3(a) is presented as a function of μ_O, while the independent variable μ_H is held at the minimum for clarity, i.e., all of the hydrogen in the system is bound to the surface. Similarly, the vibrational contributions to the energies are not included in Fig. 3(a) because they increase linearly with temperature and μ_O is a function of temperature and pressure. The magnitude of the effect of vibrational entropy (and, to a minor extent, enthalpy) at finite temperatures varies for each surface depending on the structure but has the greatest impact for the hydroxylated surfaces as shown in Table IV. For the stoichiometric surface, these vibrational energy contributions lower the surface free energy by 14 meV/Å^2 at 298.15 K and by 62 meV/Å^2 at 600 K. Because Fig. 3(a) does not incorporate these effects, it offers a first-order approximation of the relative stabilities of the surfaces studied. Yet, the data given in Table IV demonstrate that the relative ordering of the surfaces generally remains unchanged.

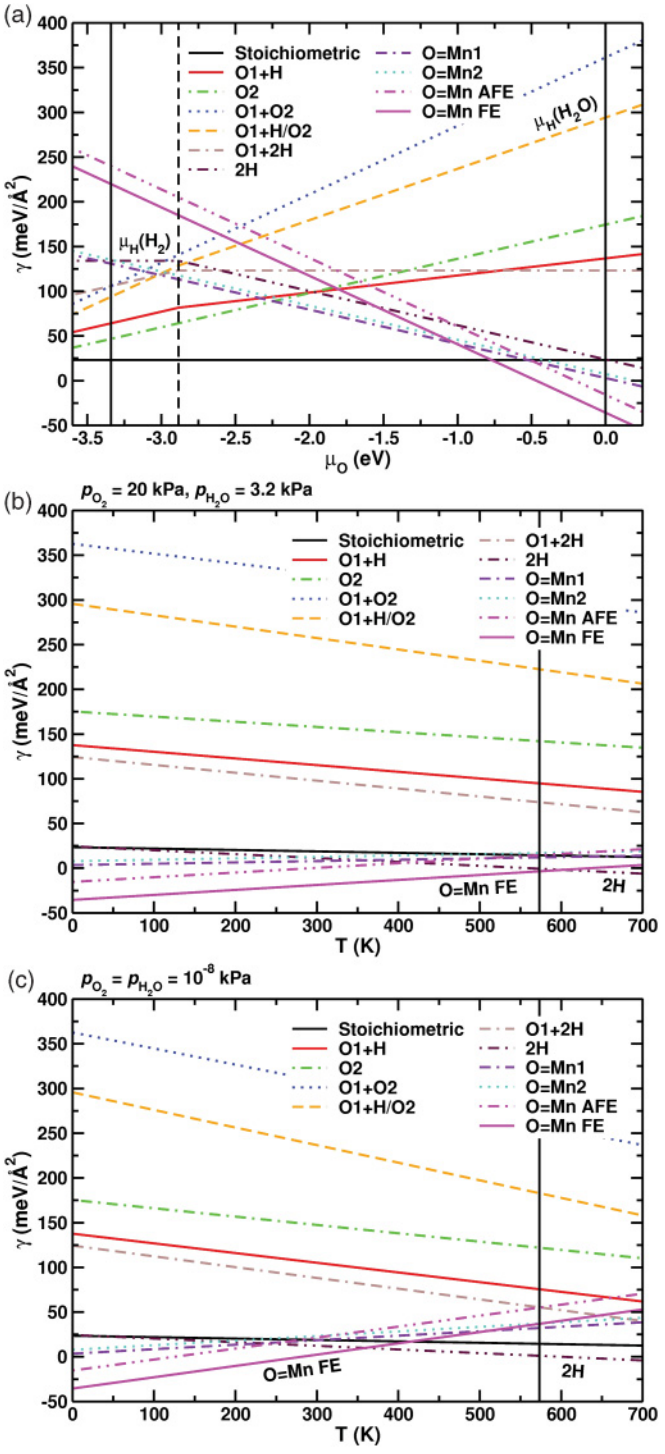

FIG. 3. (Color online) Surface free energies of various surface terminations of the γ-MnOOH (010) surface as determined by *ab initio* thermodynamics (a) as a function of μ_O at minimum μ_H and as a function of temperature at (b) p_{O_2} = 20 kPa and p_{H_2O} = 3.2 kPa and (c) $p_{O_2} = p_{H_2O} = 10^{-8}$ kPa. In (a), the vertical solid black lines bracket the range of accessible μ_O values as defined in the text. The vertical dashed black line indicates the crossover between equilibrium with H_2 and equilibrium with H_2O. In (b) and (c), the vertical black line indicates the temperature (573 K) at which γ-MnOOH oxidizes to β-MnO_2 in air.[28]

TABLE IV. Calculated enthalpy and entropy contributions to γ at different temperatures for various surface terminations of the γ-MnOOH (010) surface.

	$T = 298.15$ K			$T = 600$ K		
Structure	H^{vib} (eV)	S^{vib} (meV/K)	G^{vib} (eV)	H^{vib} (eV)	S^{vib} (meV/K)	G^{vib} (eV)
Stoichiometric	0.96	5.68	−0.73	3.15	10.7	−3.26
O1 + H	0.94	5.72	−0.77	2.97	10.4	−3.25
O2	0.95	5.75	−0.76	3.06	10.6	−3.27
O1 + O2	0.99	6.37	−0.91	3.02	11.0	−3.59
O1 + H/O2	0.97	6.42	−0.94	2.93	10.9	−3.60
O1 + 2H	0.91	5.50	−0.73	2.88	10.0	−3.12
2H	0.92	5.29	−0.66	3.01	10.1	−3.03
O = Mn1	1.04	6.30	−0.83	3.39	11.6	−3.60
O = Mn2	1.04	6.24	−0.82	3.37	11.6	−3.57
O = Mn AFE	1.09	6.52	−0.86	3.54	12.1	−3.73
O = Mn FE	1.07	6.30	−0.81	3.54	11.9	−3.62

In Figs. 3(b) and 3(c), the surface free energies, including vibrational energy, are shown at two state points that reflect μ_H values under ambient and UHV conditions, where temperature effects for all species are included.

At minimum μ_H, the stoichiometric surface is the most stable surface over a significant portion of the range of accessible μ_O [Fig. 3(a)]. Removing structural H_2O from the surface (O1 + 2H) leads to a surface 100 meV/Å^2 higher in γ than the stoichiometric surface. None of the reduced surfaces becomes stable within the range of accessible μ_O. This result is reasonable, given the fact that, at *p*H 7, thermodynamics dictates that Mn^{II} would dissolve from the surface at low p_{O_2} or be reoxidized at high p_{O_2}.[31] It should be noted, however, that we have studied limiting cases, and there may exist reduced surfaces with lower vacancy concentrations that are thermodynamically stable at low μ_O. The O = Mn FE surface, where both Mn1 and Mn2 atoms are oxidized, is predicted to be more stable than the stoichiometric one above a μ_O value of −0.77 eV. This fully oxidized surface is slightly more stable than structures where only one surface Mn is oxidized. At the crossover point, the O = Mn1 and O = Mn2 surfaces, respectively, are only 9.34 and 13.7 meV/Å^2 higher in γ. These results show that Mn1 is somewhat easier to oxidize than Mn2. Mn2 cannot donate electrons as readily as Mn1 because Mn2 has three O^{2-} in its coordination sphere, which strongly pull electrons away from it. Mn1, on the other hand, has only two O^{2-} in its coordination sphere.

In Fig. 3(b), γ is plotted as a function of temperature at ambient conditions, modeled as $p_{O_2} = 20$ kPa and $p_{H_2O} = 3.2$ kPa. The O = Mn FE surface is found to be stable up to 603 K. Above this temperature, the 2H surface becomes the most thermodynamically stable surface. The gain in entropy by driving H_2 from the surface causes the crossover from the O = Mn FE surface to the 2H surface. The predicted temperature at which hydrogen can be removed from the surface is only 30 K higher than the temperature (573 K) at which γ-MnOOH oxidizes to β-MnO_2 in air.[28] UHV conditions are also studied using $p_{O_2} = p_{H_2O} = 10^{-8}$ kPa. In Fig. 3(c), it is shown that the crossover temperature between the O = Mn FE and 2H surfaces simply shifts to lower values. The O = Mn FE surface may be observed up to a temperature of 359 K, while the 2H surface is the most stable above 359 K. Oku *et al.*[39] detected dehydration of the γ-MnOOH surface at room temperature in a vacuum system with a p_{O_2} below approximately 10^{-13} kPa. If UHV conditions are modeled as $p_{O_2} = p_{H_2O} = 10^{-13}$ kPa, then the 2H surface is calculated to be slightly lower in γ than the O = Mn FE surface at 298.15 K, which is consistent with the experimental observations. It should be noted that the stoichiometric, O = Mn1, and O = Mn2 surfaces are less than 20 meV/Å^2 higher in γ than the O = Mn FE surface at the transition to the 2H surface under all conditions simulated here and may be accessible, depending on surface preparation methods and kinetic effects. Given the limited number of surface terminations explored in this work, we must also point out that other surface terminations not discussed here may be observed experimentally. The redox behavior of the γ-MnOOH (010) surface may be richer than indicated by these results.

Of the surface reconstructions examined above, detailed structural analysis will only be provided for the O = Mn and 2H surfaces because these surfaces are predicted to be the most stable under ambient conditions. Unlike the stoichiometric AFE and FE surfaces, the O = Mn AFE and FE surfaces exhibit substantially different reconstructions [Figs. 4(a) and 4(b)], explaining the large difference in their γ values, which is not observed for other AFE and FE surface pairs. On both O = Mn surfaces, manganyl (Mn = O) groups are formed. As shown in Figs. 4(c) and 4(d), the Mn1-O bond length is 1.55 Å on both surfaces, comparable to bond lengths calculated for manganyl groups on β-MnO_2 (110), (100), and (101) oxidized surfaces[67] and for ferryl groups on the α-Fe_2O_3 (0001) surface.[71] The Mn2-O bond lengthens from 1.62 Å on the AFE surface to 1.70 Å on the FE surface. This increase in Mn2-O bond length results from the formation of hydrogen bonds between the manganyl oxygen and the hydrogens of the OH groups at the surface [see Fig. 4(d)], which pull the oxygen away from Mn2. These hydrogen-bonding interactions confer significant stabilization to the O = Mn FE surface relative to the O = Mn AFE surface. They also affect the degree of oxidation of surface and subsurface manganese. On the AFE surface, Mn1 and Mn2 are oxidized to Mn^{V} with Mn1 adopting a no-spin configuration and Mn2 assuming a

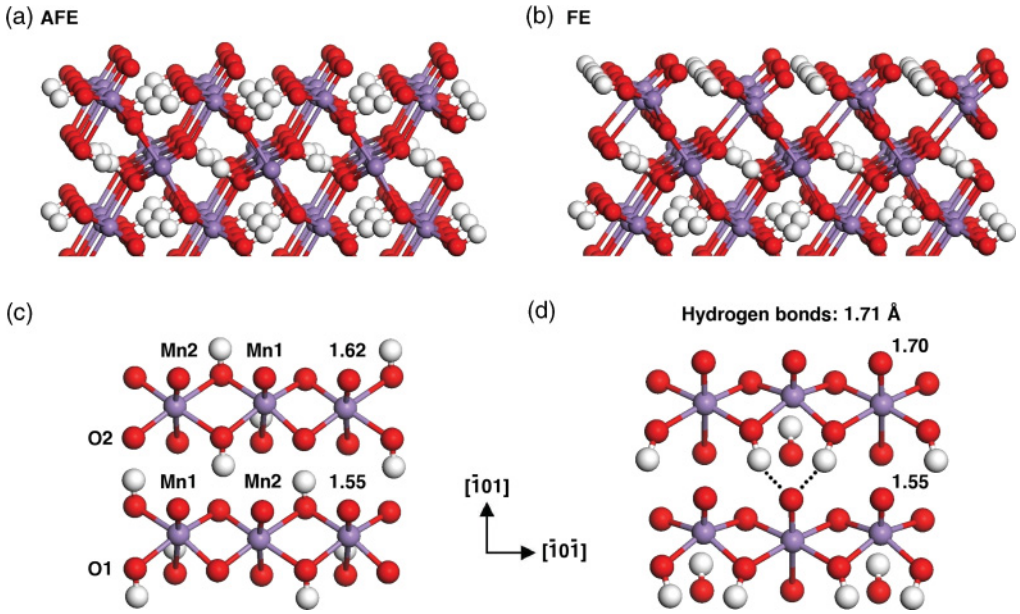

FIG. 4. (Color online) γ-MnOOH (010) O = Mn (a) AFE and (b) FE surfaces viewed along the [101] direction, (c) AFE and (d) FE surfaces viewed from the top along the [010] direction showing manganyl bond lengths in angstroms. Hydrogen bonds formed on the FE surface are illustrated with dotted lines in (d). [Mn, purple (light) sphere; O, red (dark) sphere; H, white sphere].

high-spin arrangement. Mn1 is no-spin Mn^{V} on the FE surface as well, but Mn2 is oxidized only to high-spin Mn^{IV}. The second electron withdrawn by the manganyl oxygen comes from layer 5 Mn1, which is oxidized to high-spin Mn^{IV}.

Vertical and lateral relaxations for the O = Mn AFE and FE surfaces are presented in Tables II and III, respectively. Equivalent layers of the two surfaces undergo vertical relaxation in the same direction, but the magnitudes vary considerably between the two surfaces. Layer 2 manganese atoms undergo significant relaxation out of the surface due to formation of the manganyl groups (Table II). As a result, the O-Mn layer 1–2 spacing is appreciably smaller compared to that of the stoichiometric surface (by an average of 0.446 Å for the AFE surface and 0.269 Å for the FE surface), while the layer 2–3 spacing grows by an average of 0.384 and 0.592 Å going from the stoichiometric AFE and FE surfaces, respectively, to the O = Mn surfaces. To facilitate hydrogen bonding on the O = Mn FE surface, layer 2 Mn1 and Mn2 experience significantly greater outward relaxations than they do on the O = Mn AFE surface (+67% vs +34% for Mn1 and +55% vs +38% for Mn2). Layer 1 oxygen atoms also undergo less inward relaxation on the FE surface (Table II). Because the hydrogen bonds between layer 1 and layer 3 are broken to form the hydrogen bonds between the manganyl oxygen and the hydrogen atoms at the surface, layer 3 oxygen atoms on the FE surface relax into the surface to a greater degree than those on the AFE surface (−29% vs −10%). Differences in the layer 5–6 Mn2-O relaxation between the AFE and FE surfaces result from the same mechanism as described for the stoichiometric surfaces. The lateral relaxations of the first two layers on the FE surface are considerably larger than those on the AFE surface (Table III). Along the [001] direction, the layer 1 and layer 2 relaxations range from +0.36 to +0.56 Å, while they span −0.25 to −0.44 Å along the [100] direction on the FE surface. These large lateral movements enable the formation of hydrogen bonds at the surface. The lateral relaxations of the remaining layers on the FE surface and of all layers on the AFE surface are less than ±0.10 Å (Table III).

The oxidized 2H surface exhibits a reconstruction visually similar to the stoichiometric surface (see Fig. 1), but significant differences in vertical and lateral relaxations exist (Tables II and III, respectively). The layer 1–2 spacing is similar to the stoichiometric FE surface with O1 and O2 expanding outward by +30% and +26%, respectively (it should be noted that layer 1 and layer 3 O1 atoms are chemically equivalent to O2 on this surface). Unlike on the stoichiometric surface, layer 2 manganese atoms undergo significant outward expansion of approximately +21% relative to the bulk, while layer 3 oxygen atoms relax toward the bulk by −32%. These changes in vertical layer spacing result from the lack of hydrogen bonding at the surface, which normally prevents layer 3 oxygen from falling toward the bulk. The layer 3 oxygen then also pulls the layer 5 manganese away from the bulk to gain more electron density from the manganese, thereby increasing the layer 5–6 spacing (Table II) and decreasing the layer 3 O-layer 5 Mn bond lengths by an average of 0.43 Å relative to the stoichiometric FE surface. The oxidation of the surface by removal of H_2 gas also causes considerable lateral relaxations throughout much of the slab (Table III). The lateral relaxations of layer 1 oxygen atoms are similar to those for the equivalent atoms on the O = Mn FE surface (Table III). Generally, the atoms shift along the [001] and [$\bar{1}$00] directions with the magnitude of the shift decreasing moving away from the surface. For the first three layers, this lateral displacement, combined with the vertical relaxations, is consistent with the formation of microfissures along the [210] direction of orthorhombic manganite observed near the transition front between γ-MnOOH and β-MnO_2 and

proposed to result from removal of hydrogen.[30] The 2H surface reconstruction, therefore, demonstrates a possible pathway to the structural rearrangement that occurs upon oxidation of γ-MnOOH to β-MnO_2. Intriguingly, the oxidation does not occur layer by layer as layer 2 Mn2 and layer 5 Mn1 are oxidized to high-spin Mn^{IV}, while the rest of the manganese atoms in the slab maintain high-spin Mn^{III} oxidation states except layer 5 Mn2, which is low-spin Mn^{III}.

C. Hydrated surfaces

Both dissociative and molecular adsorption of H_2O at half-monolayer and monolayer coverages on the γ-MnOOH (010) stoichiometric surface were investigated to examine completion of the surface manganese coordination sphere due to hydration. A combination of the two adsorption mechanisms was not pursued because molecular adsorption is significantly more favorable than dissociative adsorption and test calculations show that the combination of the two results in energies comparable to dissociative adsorption alone. A total of 22 and 11 initial positions were optimized for half-monolayer and monolayer coverages, respectively. It should be noted that, although a large number of configurations of water molecules were examined, it is possible that the global minima may not have been located and lower-energy structures than those presented here are possible. At half-monolayer coverage, H_2O is considered to adsorb only on Mn1 or Mn2. The naming scheme used here reflects the type of adsorption and the surface manganese on which H_2O adsorbs. The set of surfaces named H_2O-Mn1 represents molecular adsorption on Mn1, and H_2O-Mn2 identifies the set of surfaces with H_2O molecularly adsorbed on Mn2. (At half-monolayer coverage, only molecular adsorption is exothermic because hydrogen-bonding interactions cannot stabilize dissociated water.) The H_2O-Mn and HO-Mn surfaces signify molecular and dissociative adsorption, respectively, at monolayer coverage (on all surface manganese).

Table V lists the adsorption energies ΔE_{ads}, γ values at minimum μ_H and maximum μ_O (excluding vibrational energy), and geometrical properties for all unique minima located. The definition of ΔE_{ads} is

$$\Delta E_{ads} = \left(E_{slab}^{H_2O} - E_{slab}^{clean} - N_{H_2O} E_{H_2O}^{gas}\right)/N_{H_2O}, \qquad (9)$$

where $E_{slab}^{H_2O}$, E_{slab}^{clean}, and $E_{H_2O}^{gas}$ are the DFT total energies of the hydrated surface slab, stoichiometric FE surface slab, and gas-phase H_2O, respectively, and N_{H_2O} is the number of adsorbed water molecules per slab. The lowest-energy AFE and FE structures are depicted in Fig. 5. At half-monolayer coverage, H_2O adsorption on Mn1 is slightly more favorable than adsorption on Mn2 (−0.60 vs −0.55 eV). This result is consistent with Mn1 being somewhat easier to oxidize due to fewer O^{2-} ligands in its coordination sphere as discussed previously. In contrast, Xia *et al.*[44] determined that Mn2 is the preferred adsorption site at quarter-monolayer coverage. Their lowest-energy structure with H_2O adsorbed on Mn1 is similar to the H_2O-Mn1 surface found here with an adsorption energy of -0.47 eV/H_2O, which has weaker hydrogen bonds between the surface oxygen and the hydrogen of the water (O1-H_w and O2-H_w) than the lowest-energy structure located in this study (see Table V). Given the error in DFT energies in this work, however, the lowest-energy H_2O-Mn1 and H_2O-Mn2 surfaces can be considered to be degenerate as their difference in γ is only 2.26 meV/Å^2. An FE arrangement of the O-H dipoles is preferred for the H_2O-Mn1 surface [Fig. 5(b)], while the H_2O-Mn2 surface has a more favorable AFE structure [Fig. 5(c)], in agreement with the results of Xia *et al.*[44] at quarter-monolayer coverage. The energetic differences between the lowest-energy AFE and FE structures, however, are essentially nonexistent. The overlayer of H_2O molecules donates hydrogen bonds to the O2 atoms at the AFE surfaces [see bond lengths in Table V and illustrations in Figs. 5(a) and 5(c)], satisfying their undersaturation enough to make the differences between the FE and the AFE surfaces insignificant energetically. This general observation holds for monolayer coverage of molecularly adsorbed water as well [H_2O-Mn; Fig. 5(e)] and agrees with the observation of Xia *et al.*[44] that the O-H dipole orientation at the surface is controlled by the local water environment. Also of note is the large number of unique structures found for half-monolayer water coverage within 5.24 meV/Å^2 of each other in γ (Table V). This small variation in γ along with the relatively long bond lengths between surface manganese and the oxygen of the adsorbed H_2O molecules O_w (Mn-O_w in Table V) demonstrates that the interaction between water and the γ-MnOOH (010) surface is weak. Therefore, surface energies of other configurations not found in this work can be expected to be similar to those listed in Table V. These results are consistent with a recent AIMD study that concluded that water-water interactions were dominant at the interface as water becomes bulklike close to the surface.[44]

Monolayer coverage of molecularly adsorbed water on the γ-MnOOH (010) surface is more favorable than half-monolayer coverage with $\Delta E_{ads} = -0.69$ eV. This result is not surprising given the additional hydrogen-bonding interactions at the surface at monolayer coverage compared to half-monolayer coverage. As shown in Figs. 5(e) and 5(f), monolayer H_2O coverage allows the formation of a hydrogen-bonding network along the [101] direction, consisting of average hydrogen-bond lengths of 1.98 and 2.09 Å. Because of the stronger water-water interactions at monolayer coverage, the Mn-O_w bonds weaken and lengthen by an average of 0.06 and 0.15 Å for Mn1 and Mn2, respectively, compared to those on surfaces with half-monolayer coverage. The oxygen atoms of the water molecules are located between 1.47 and 1.52 Å above layer 1. On the H_2O-Mn AFE surface, the water molecules are closer to the surface to allow for stronger hydrogen bonding between adsorbed H_2O and two-fold coordinated oxygen at the surface (Table II). Therefore, the hydrogen bonds and Mn-O_w bonds are generally shorter on the AFE surface than on the FE surface and give rise to smaller vertical relaxations at the AFE surface (see Table II). Similar to the stoichiometric surfaces, layer 1 oxygen and layer 2 manganese undergo outward and inward relaxations, respectively, relative to the bulk, but the magnitudes of the relaxations are reduced nearly in half (see Table II). The layer of H_2O molecules confines the layer 1 oxygen atoms closer to the surface, while the weak Mn-O_w interaction pulls the layer 2 manganese out of the surface relative to the stoichiometric surface. Small lateral relaxations are experienced throughout

TABLE V. Calculated properties of water adsorbed on the γ-MnOOH (010) surface.

Structure	Surface OH ordering	ΔE_{ads} (eV/H_2O)	γ[a] (meV/Å^2)	$R_{Mn\text{-}O_w}$ (Å)	$R_{O1\text{-}H_w}$[b] (Å)	$R_{O2\text{-}H_w}$[c] (Å)	$R_{O_w\text{-}H_w}$[d] (Å)
H_2O-Mn1	FE	−0.60	−0.028	2.39	2.41	1.93	
	AFE	−0.60	−0.003	2.35	2.47	1.80	
	FE	−0.59	0.405	2.39	2.55	2.02	
	FE	−0.58	0.781	2.41	2.57	2.07	
	AFE	−0.58	1.07	2.37	2.59	1.87	
	FE	−0.47	5.21	2.49	2.16	2.19	
H_2O-Mn2	AFE	−0.55	2.23	2.38	2.60	1.83	
	FE	−0.54	2.41	2.43	2.10	2.49	
	FE	−0.54	2.46	2.44	2.63	1.95	
	FE	−0.54	2.48	2.44	1.96	2.45	
	AFE	−0.52	3.02	2.40	2.57	1.90	
	AFE[e]	−0.49	4.18	2.41	1.91	2.56	
H_2O-Mn[f]	FE	−0.69	−29.6	2.48	2.39	2.22	2.07
				2.58	2.20	2.42	1.98
	AFE	−0.68	−28.7	2.45	2.41	2.13	2.10
				2.55	2.18	2.40	1.97
HO-Mn[f]	FE	−0.31	−0.931	1.87			2.05
				1.88			1.98

[a] γ is given for minimum μ_H and maximum μ_O, excluding vibrational energy.
[b] Structurally equivalent to O1 in the bulk but chemically equivalent to O2 for the HO-Mn surface.
[c] Structurally equivalent to O2 in the bulk but chemically equivalent to O1 for FE surfaces.
[d] Distances between adjacent H_2O molecules in the hydrogen-bonding network along the [101] direction.
[e] Surface O1 and O2 switch identities.
[f] Values in first and second rows are for H_2O or OH^- adsorbed on Mn1 and Mn2, respectively.

much of the H_2O-Mn AFE and FE surface slabs, as observed for the stoichiometric surfaces (Table III).

Although dissociated water cannot be stabilized at half-monolayer coverage, the hydrogen-bonding network along the [101] direction at monolayer coverage overcompensates for the unfavorable energetics of dissociation [Fig. 5(g)]. Formation of the HO-Mn surface is exothermic with a ΔE_{ads} value of −0.31 eV, which is still significantly higher than that for molecularly adsorbed water in both low- and high-coverage regimes (see Table V). An earlier investigation of γ-MnOOH (010) hydrated surfaces did not find a stable structure for dissociatively adsorbed H_2O.[44] Because of the extra hydrogen atoms atop each layer 1 oxygen atom, all structural protons are transferred from layer 1 oxygen to layer 3 oxygen, and only an FE arrangement of O-H dipoles is found at the HO-Mn surface. The adsorbed OH^- groups are chemisorbed to surface manganese as demonstrated by Mn-O_w bond lengths of 1.87-1.88 Å, completing the coordination sphere of surface manganese. Only when water dissociates at the surface is the coordination sphere of surface manganese truly completed. These strong bonds along with the atop hydrogen atoms on layer 1 oxygen lead to a considerably different surface reconstruction compared to the clean stoichiometric FE surface. Similar to the O = Mn surfaces, layer 1 oxygen atoms undergo inward relaxations, although to a much smaller degree (approximately −5% relative to the bulk). The adsorption of OH^- groups on layer 2 manganese results in the manganese moving out of the surface relative to the stoichiometric FE surface (Table II), but layer 2 Mn1 still experiences a small inward relaxation of −4% relative to the bulk. Layer 2 Mn2 relaxes out of the surface by +7%. Large vertical relaxations are observed for layer 3 and layer 4 oxygen atoms (−12% and +13%, respectively). Layer 1 oxygen and layer 2 Mn1 undergo significant lateral relaxations along the [10$\bar{1}$] direction (Table III), which lead to stronger hydrogen bonds between layer 1 oxygen and layer 3 OH^- groups than those between layer 1 OH^- groups and layer 3 oxygen on the stoichiometric FE surface (1.49 vs 1.65 Å). Layer 2 Mn2 and layer 3 oxygen also experience lateral movement of greater than 0.10 Å along the [00$\bar{1}$] direction. Lateral relaxations of layers below layer 3 are generally small (Table III).

In Fig. 6, the results of *ab initio* thermodynamics calculations are shown for the lowest-energy stoichiometric, H_2O-Mn1, H_2O-Mn2, H_2O-Mn, and HO-Mn surfaces. Figure 6(a) shows that, even at the minimum μ_H, all hydrated surfaces are significantly lower in γ than the stoichiometric surface. The H_2O-Mn surface is predicted to be the most stable surface over the entire range of accessible μ_O, and the next lowest-energy surface, the HO-Mn surface, is 28.6 meV/Å^2 higher in γ when the surface is in equilibrium with H_2O. Interestingly, the HO-Mn surface is essentially degenerate in energy with the H_2O-Mn1 and H_2O-Mn2 surfaces given the uncertainty in the calculations, although ΔE_{ads} is much lower for molecular adsorption at half-monolayer coverage than for dissociative adsorption at monolayer coverage (−0.60 and −0.55 eV vs −0.31 eV). The difference in γ values between surfaces with molecularly adsorbed H_2O at half-monolayer and monolayer coverages is also considerably larger than their similar adsorption energies would indicate (see Table V). These results demonstrate the large impact hydrogen bonding can have on calculated γ values, leading to predictions of stable surface terminations that differ from those obtained with simple adsorption energies alone. Surface free energies at finite temperatures and pressures for μ_H shown in

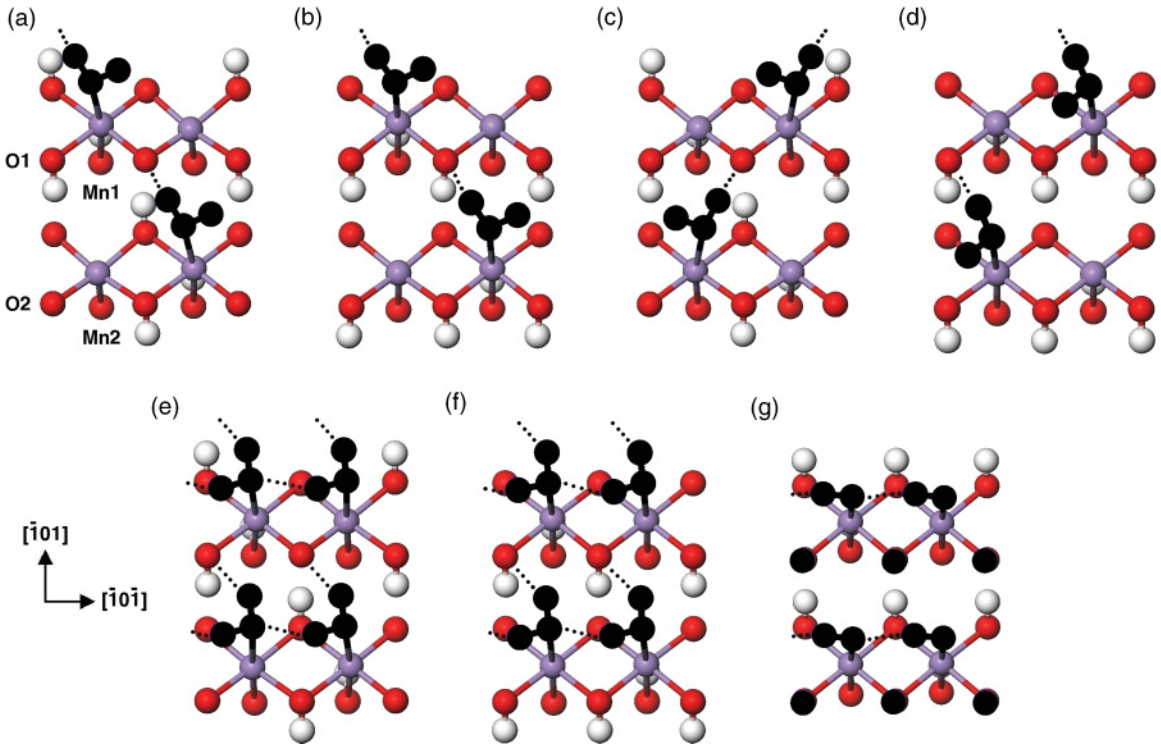

FIG. 5. (Color online) Lowest-energy γ-MnOOH (010) hydrated surfaces viewed from the top along the [010] direction with oxygen and hydrogen atoms of adsorbed H_2O, OH^-, and H^+ species pictured as black spheres: H_2O-Mn1 (a) AFE and (b) FE surfaces, H_2O-Mn2 (c) AFE and (d) FE surfaces, H_2O-Mn (e) AFE and (f) FE surfaces, (g) HO-Mn FE surface. Hydrogen bonds are illustrated with dotted lines. [Mn, purple (light gray) sphere; structural O, red (dark gray) sphere; structural H, white sphere].

Figs. 6(b) and 6(c), however, provide results more in line with ΔE_{ads} as hydrogen bonding is destabilized by entropy and vibrational motions with increasing temperature. At ambient conditions [p_{O_2} = 20 kPa, p_{H_2O} = 3.2 kPa; Fig. 6(b)], the H_2O-Mn surface is predicted to be the most thermodynamically stable up to a temperature of 434 K, above which water is driven off the surface to give the stoichiometric surface. The H_2O-Mn1 and H_2O-Mn2 surfaces, respectively, are only 3.15 and 5.24 meV/Å^2 higher in γ at the crossover point, which is more consistent with the comparable ΔE_{ads} values for those surfaces and the H_2O-Mn surface. The low p_{O_2} and p_{H_2O} of 10^{-8} kPa used to model UHV conditions shifts the crossover from the H_2O-Mn surface to the stoichiometric surface to a temperature of 284 K [Fig. 6(c)]. Again, the H_2O-Mn1 and H_2O-Mn2 surfaces are close in γ at the intersection temperature.

D. Comparison of oxidized and hydrated surface terminations

Figure 7 combines the *ab initio* thermodynamics results for the most stable surface terminations. Under ambient conditions [Fig. 7(a)] and under UHV [Fig. 7(b)], the O = Mn FE surface is predicted to be observed, followed by a transition to the surface oxidized by H_2 removal (the 2H surface). The fully hydrated H_2O-Mn surface is only 6.23 meV/Å^2 higher in γ than the O = Mn FE surface at 0 K, but this difference grows rapidly as the temperature increases. At 298.15 K and ambient conditions, 21.1 meV/Å^2 in γ separates the O = Mn FE and H_2O-Mn surfaces, and the hydrated surface may be accessible, depending on surface preparation. It is possible that a hydrated surface with γ lower than that of the oxidized surfaces exists but is not located in the present study, although the weak coordination of the water oxygens to the surface manganese suggests different configurations of water would not have a significant impact on γ. The stoichiometric surface is increasingly accessible as a metastable state with increasing temperature (Fig. 7). These results generally indicate that γ-MnOOH (010) oxidized surfaces should be observed experimentally, in agreement with the fact that aging of natural γ-MnOOH is known to involve oxidation to β-MnO_2.[29,30,32,33] Yet, most XPS studies have assigned a 3+ oxidation state to manganese at γ-MnOOH single crystal[31,35] and powder[35,36] surfaces. Only under acid treatment has Mn^{IV} been detected at the surface.[38] It is, however, interesting that O 1*s* spectra are more consistent with the oxidized surfaces as they have indicated that water content at the surface is low (or nonexistent) compared to O^{2-} and OH^- content.[35,36,38] The O = Mn FE surface has an O^{2-}:OH^- ratio of 1:1 at the surface, which has been found in a few XPS studies.[35,37] Because it is unclear which surfaces were examined and what surface preparation techniques were used in some of the experimental work, direct comparison of the calculated results with experimental data should be made with caution. The method by which a surface is prepared is known to have a strong influence on the observed surface structure because kinetic effects can essentially trap a surface in a metastable state. An early report by Hem and Lind[33] demonstrated that, while γ-MnOOH is less

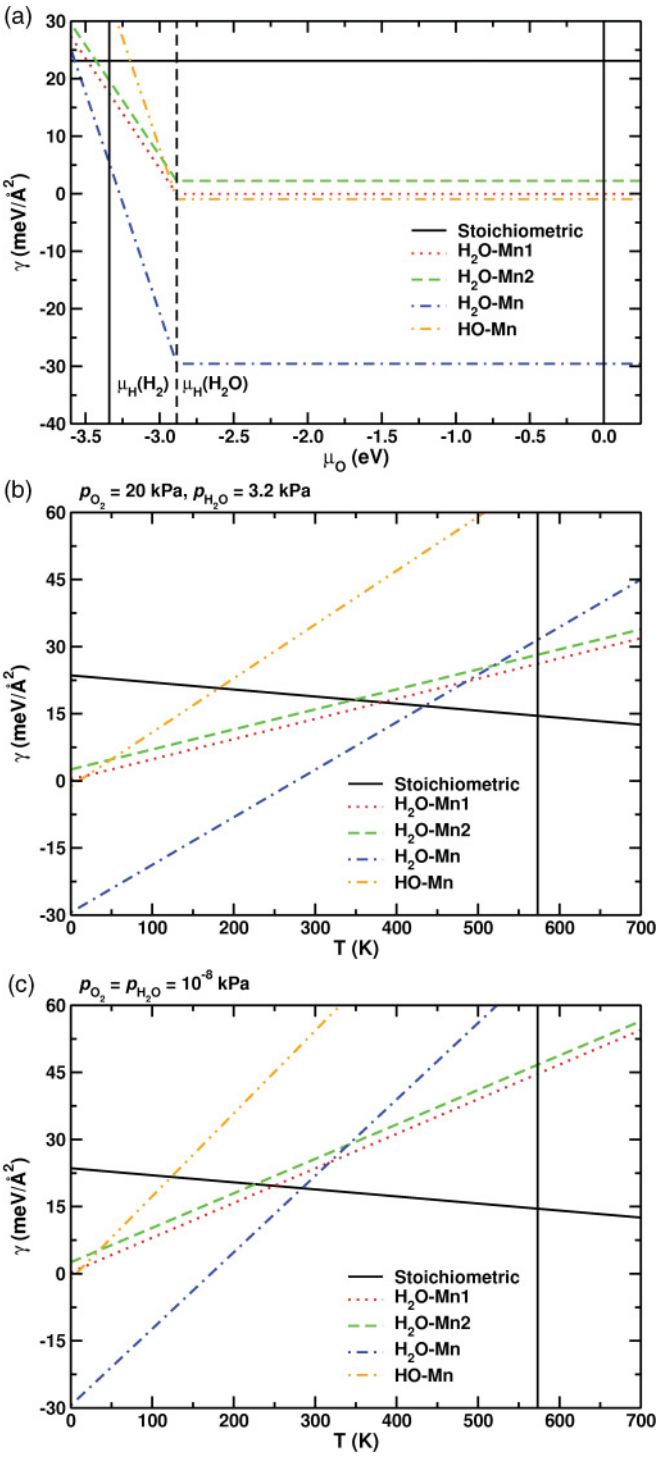

FIG. 6. (Color online) Surface free energies of hydrated γ-MnOOH (010) surfaces as determined by *ab initio* thermodynamics (a) as a function of μ_O at minimum μ_H and as a function of temperature at (b) $p_{O_2} = 20$ kPa and $p_{H_2O} = 3.2$ kPa and (c) $p_{O_2} = p_{H_2O} = 10^{-8}$ kPa. Only the lowest-energy surface for each coverage regime and type of adsorption is shown. In (a), the vertical solid black lines bracket the range of accessible μ_O values as defined in the text. The vertical dashed black line indicates the crossover between equilibrium with H_2 and equilibrium with H_2O. In (b) and (c), the vertical black line indicates the temperature (573 K) at which γ-MnOOH oxidizes to β-MnO_2 in air.[28]

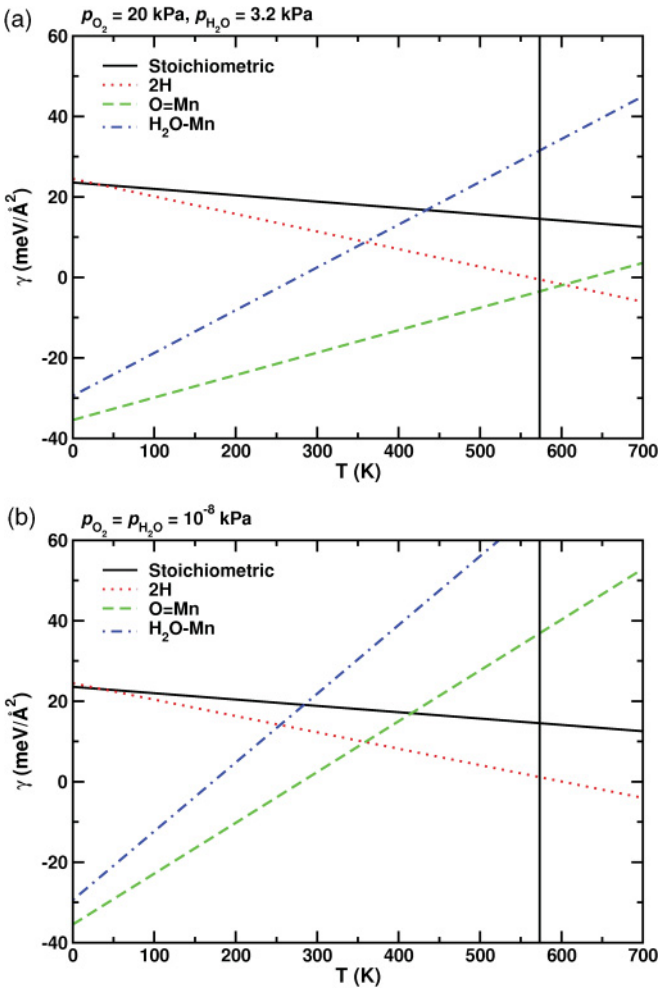

FIG. 7. (Color online) Surface free energies of the lowest-energy γ-MnOOH (010) surfaces as determined by *ab initio* thermodynamics as a function of temperature at (a) $p_{O_2} = 20$ kPa and $p_{H_2O} = 3.2$ kPa and (b) $p_{O_2} = p_{H_2O} = 10^{-8}$ kPa. The vertical black line indicates the temperature (573 K) at which γ-MnOOH oxidizes to β-MnO_2 in air.[28]

stable than higher oxides, aging through disproportionation is kinetically controlled and slow. Therefore, the experimental data on γ-MnOOH surfaces collected to date may represent metastable surfaces that are kinetically trapped rather than the most thermodynamically stable surface. Given the Mn^{III} oxidation state and the low water content on a number of these surfaces, they are likely partially hydrated stoichiometric surfaces. Because the present study ranks only thermodynamic stability, an oxidized surface is predicted to be observed in the absence of kinetic limitations. The results of the present work can be used to explain experimental structural analyses and to identify the metastable states that persist in precisely controlled environments.

IV. CONCLUSIONS

The γ-MnOOH (010) surface was studied using *ab initio* thermodynamics, with a particular emphasis on identifying stable surface terminations, exploring the redox behavior of the

surface, and investigating hydration of the clean stoichiometric surface. While the clean stoichiometric surface has a low surface energy, it may only be observed as a metastable state in experiments. Instead, oxidized surfaces are predicted to be the most thermodynamically stable surfaces under environmentally relevant conditions. The O = Mn FE surface is particularly stable due to the formation of hydrogen bonds between surface manganyl groups and structural hydrogen. Under ambient conditions, the crossover temperature from the O = Mn FE surface to the 2H surface closely matches the temperature at which γ-MnOOH oxidizes to β-MnO_2 in air (603 vs 573 K). The 2H surface reconstruction may give insight into the initial oxidation steps for this process. Reduced surfaces are not found to be stable even under severely reducing conditions (low μ_O).

While the bulk exhibits AFE arranged O-H dipoles, an FE configuration is more stable when undersaturated oxygen atoms are present at the surface. Hydrogen transfer to these two-fold coordinated oxygen atoms leads to energetic gains of no greater than 8 meV/Å^2 in most cases. On the O = Mn FE surface, however, the hydrogen-bonding interactions between the manganyl groups and structural hydrogen result in a decrease in γ of 20.1 meV/Å^2 relative to the O = Mn AFE surface when vibrational energy is neglected (inclusion of vibrational energy leads to a slight decrease in this difference with increasing temperature). When the stoichiometric surface is hydrated, hydrogen bonds donated from the adsorbed water molecules stabilize the AFE surfaces so that they become essentially degenerate with the FE surfaces.

The hydration results presented in this work are generally consistent with an earlier AIMD study of water at the γ-MnOOH (010) surface.[44] The weak interactions between molecularly adsorbed H_2O and the surface are demonstrated by long Mn-O_w bonds and small energetic differences between a large number of surfaces with half-monolayer coverage. Molecular adsorption at monolayer coverage is considerably more stable than half-monolayer coverage due to the formation of a hydrogen-bonding network along the [101] direction. This hydrogen-bonding network is also able to stabilize dissociatively adsorbed water at monolayer coverage. In the absence of hydrogen-bonding interactions at half-monolayer coverage, water is unable to dissociate. While the hydrated surfaces are significantly lower in γ than the stoichiometric surface at low temperatures and ambient p_{O_2} and p_{H_2O}, they are less thermodynamically stable than the oxidized surfaces at finite temperatures. As with the clean stoichiometric surface, the H_2O-Mn surface is likely accessible as a metastable state, especially in light of experimental evidence for strong kinetic limitations to oxidation of the surface under environmentally relevant conditions. Therefore, the structural details for the most stable unoxidized surfaces presented in this work may be useful in the interpretation of experimental results.

ACKNOWLEDGMENTS

This work used the high-performance computing resources of the Raritan cluster at the National Institute of Standards and Technology, the Helix Systems Biowulf cluster at the National Institutes of Health, and the Arctic Region Supercomputing Center at the University of Alaska Fairbanks. G.A.E.O. was supported by the National Research Council. The authors would like to thank Professor Sara Mason, Professor Tom Trainor, Dr. Peter Eng, and Dr. Joanne Stubbs for useful discussions.

[1] S. L. Brock, N. Duan, Z. R. Tian, O. Giraldo, H. Zhou, and S. L. Suib, Chem. Mater. **10**, 2619 (1998).
[2] N. D. Ivanova, S. V. Ivanov, E. I. Boldyrev, G. V. Sokol'skii, and I. S. Makeeva, Russ. J. Appl. Chem. **75**, 1420 (2002).
[3] Y. F. Han, L. Chen, K. Ramesh, E. Widjaja, S. Chilukoti, I. K. Surjami, and J. Chen, J. Catal. **253**, 261 (2008).
[4] X. F. Tang, J. H. Li, L. A. Sun, and J. M. Hao, Appl. Catal., B **99**, 156 (2010).
[5] D. Balachandran, D. Morgan, G. Ceder, and A. van de Walle, J. Solid State Chem. **173**, 462 (2003).
[6] Y. L. Cao, H. X. Yang, X. P. Ai, and L. F. Xiao, J. Electroanal. Chem. **557**, 127 (2003).
[7] D. Liu, J. J. Sansalone, and F. K. Cartledge, J. Environ. Eng. **131**, 1178 (2005).
[8] M. M. Ahammed and V. Meera, J. Hazard. Mater. **181**, 788 (2010).
[9] X. Cao, N. Wang, L. Wang, C. Mo, Y. Xu, X. Cai, and L. Guo, Sens. Actuators B **147**, 730 (2010).
[10] R. M. McKenzie, Soil Res. **18**, 61 (1980).
[11] L. E. Eary and D. Rai, Environ. Sci. Technol. **21**, 1187 (1987).
[12] H. W. Nesbitt, G. W. Canning, and G. M. Bancroft, Geochim. Cosmochim. Acta **62**, 2097 (1998).
[13] L. Bochatay and P. Persson, J. Colloid Interface Sci. **229**, 593 (2000).
[14] L. Bochatay, P. Persson, and S. Sjoberg, J. Colloid Interface Sci. **229**, 584 (2000).
[15] C. A. Johnson and A. G. Xyla, Geochim. Cosmochim. Acta **55**, 2861 (1991).
[16] S. E. Fendorf, M. Fendorf, D. L. Sparks, and R. Gronsky, J. Colloid Interface Sci. **153**, 37 (1992).
[17] S. E. Fendorf and R. J. Zasoski, Environ. Sci. Technol. **26**, 79 (1992).
[18] A. Manceau and L. Charlet, J. Colloid Interface Sci. **148**, 425 (1992).
[19] E. Silvester, L. Charlet, and A. Manceau, J. Phys. Chem. **99**, 16662 (1995).
[20] P. S. Nico and R. J. Zasoski, Environ. Sci. Technol. **34**, 3363 (2000).
[21] R. M. Weaver, M. F. Hochella, and E. S. Ilton, Geochim. Cosmochim. Acta **66**, 4119 (2002).
[22] V. Q. Chiu and J. G. Hering, Environ. Sci. Technol. **34**, 2029 (2000).
[23] B. A. Manning, S. E. Fendorf, B. Bostick, and D. L. Suarez, Environ. Sci. Technol. **36**, 976 (2002).
[24] A. L. Foster, G. E. Brown, and G. A. Parks, Geochim. Cosmochim. Acta **67**, 1937 (2003).
[25] M. Q. Zhu, K. W. Paul, J. D. Kubicki, and D. L. Sparks, Environ. Sci. Technol. **43**, 6655 (2009).
[26] M. J. Buerger, Z. Kristallogr. **95**, 163 (1936).
[27] H. Dachs, Z. Kristallogr. **118**, 303 (1963).

[28]T. Kohler, T. Armbruster, and E. Libowitzky, J. Solid State Chem. **133**, 486 (1997).
[29]J. H. Rask and P. R. Buseck, Am. Mineral. **71**, 805 (1986).
[30]M. Amouric, S. Parc, and D. Nahon, Clays Clay Miner. **39**, 254 (1991).
[31]Y. S. Jun and S. T. Martin, Environ. Sci. Technol. **37**, 2363 (2003).
[32]O. Bricker, Am. Mineral. **50**, 1296 (1965).
[33]J. D. Hem and C. J. Lind, Geochim. Cosmochim. Acta **47**, 2037 (1983).
[34]D. B. Loomer, T. A. Al, L. Weaver, and S. Cogswell, Am. Mineral. **92**, 72 (2007).
[35]H. W. Nesbitt and D. Banerjee, Am. Mineral. **83**, 305 (1998).
[36]J. J. Rosso and M. F. Hochella, Surf. Sci. Spectra **4**, 253 (1996).
[37]S. Ardizzone, C. L. Bianchi, and D. Tirelli, Colloids Surf., A **134**, 305 (1998).
[38]M. Ramstedt, A. V. Shchukarev, and S. Sjoberg, Surf. Interface Anal. **34**, 632 (2002).
[39]M. Oku, K. Hirokawa, and S. Ikeda, J. Electron Spectrosc. Relat. Phenom. **7**, 465 (1975).
[40]M. Batzill, K. Katsiev, J. M. Burst, U. Diebold, A. M. Chaka, and B. Delley, Phys. Rev. B **72**, 165414 (2005).
[41]C. S. Lo, K. S. Tanwar, A. M. Chaka, and T. P. Trainor, Phys. Rev. B **75**, 075425 (2007).
[42]P. M. Kowalski, B. Meyer, and D. Marx, Phys. Rev. B **79**, 115410 (2009).
[43]S. E. Mason, C. R. Iceman, T. P. Trainor, and A. M. Chaka, Phys. Rev. B **81**, 125423 (2010).
[44]S. W. Xia, G. Pan, Z. L. Cai, Y. Wang, and J. R. Reimers, J. Phys. Chem. C **111**, 10427 (2007).
[45]B. Delley, J. Chem. Phys. **92**, 508 (1990).
[46]B. Delley, J. Chem. Phys. **113**, 7756 (2000).
[47]J. P. Perdew, K. Burke, and M. Ernzerhof, Phys. Rev. Lett. **77**, 3865 (1996).
[48]H. J. Monkhorst and J. D. Pack, Phys. Rev. B **13**, 5188 (1976).
[49]H. Dachs, Int. J. Magn. **4**, 5 (1973).
[50]D. Balachandran, D. Morgan, and G. Ceder, J. Solid State Chem. **166**, 91 (2002).
[51]V. I. Anisimov, J. Zaanen, and O. K. Andersen, Phys. Rev. B **44**, 943 (1991).
[52]C. J. Cramer and D. G. Truhlar, Phys. Chem. Chem. Phys. **11**, 10757 (2009).
[53]C. Franchini, V. Bayer, R. Podloucky, J. Paier, and G. Kresse, Phys. Rev. B **72**, 045132 (2005).
[54]C. Franchini, V. Bayer, R. Podloucky, G. Parteder, S. Surnev, and F. P. Netzer, Phys. Rev. B **73**, 155402 (2006).
[55]V. Bayer, C. Franchini, and R. Podloucky, Phys. Rev. B **75**, 035404 (2007).
[56]C. Franchini, R. Podloucky, J. Paier, M. Marsman, and G. Kresse, Phys. Rev. B **75**, 195128 (2007).
[57]S. A. Prosandeev, E. Cockayne, B. P. Burton, S. Kamba, J. Petzelt, Y. Yuzyuk, R. S. Katiyar, and S. B. Vakhrushev, Phys. Rev. B **70**, 134110 (2004).
[58]X.-G. Wang, W. Weiss, S. K. Shaikhutdinov, M. Ritter, M. Petersen, F. Wagner, R. Schlogl, and M. Scheffler, Phys. Rev. Lett. **81**, 1038 (1998).
[59]X.-G. Wang, A. Chaka, and M. Scheffler, Phys. Rev. Lett. **84**, 3650 (2000).
[60]K. Reuter and M. Scheffler, Phys. Rev. B **65**, 035406 (2002).
[61]C. Stampfl, M. V. Ganduglia-Pirovano, K. Reuter, and M. Scheffler, Surf. Sci. **500**, 368 (2002).
[62]K. Reuter and M. Scheffler, Phys. Rev. B **68**, 045407 (2003).
[63]K. Reuter and M. Scheffler, Phys. Rev. Lett. **90**, 046103 (2003).
[64]Q. Sun, K. Reuter, and M. Scheffler, Phys. Rev. B **67**, 205424 (2003).
[65]W. Bergermayer and I. Tanaka, Appl. Phys. Lett. **84**, 909 (2004).
[66]T. P. Trainor, A. M. Chaka, P. J. Eng, M. Newville, G. A. Waychunas, J. G. Catalano, and G. E. Brown, Surf. Sci. **573**, 204 (2004).
[67]G. A. E. Oxford and A. M. Chaka, J. Phys. Chem. C **115**, 16992 (2011).
[68]D. A. McQuarrie, *Statistical Mechanics* (University Science, Sausalito, CA, 2000).
[69]*NIST-JANAF Thermochemical Tables*, 4th ed., edited by J. Chase (American Chemical Society, Washington, DC, 1998).
[70]D. Hobbs, J. Hafner, and D. Spisak, Phys. Rev. B **68**, 014407 (2003).
[71]E. A. Jarvis and A. M. Chaka, Surf. Sci. **601**, 1909 (2007).